fibers

MDPI

Article

Bond Stress Analysis Between High-Performance Steel Fiber Reinforced Mortar and Deformed Steel Bars Under Pull-Out Test

Ramdane Sidali Amrouche [1], Samira Djaknoun [1], Messaoud Saidani [2,*], Zineb Abeoub [1] and Giangiacomo Minak [3]

[1] Laboratory of Advanced Mechanics (LMA), University of Sciences and Technology Houari Boumediene (USTHB), Algiers 16111, Algeria; ramrouche@usthb.dz (R.S.A.); samira.djaknoun@usthb.edu.dz (S.D.); zabeoub@usthb.dz (Z.A.)
[2] Research Centre for Manufacturing and Materials, Coventry University, Priory Street, Coventry CV1 5FB, UK
[3] Department of Industrial Engineering, University of Bologna, Via Luciano Montaspro, 97, 47121 Forlì, Italy; giangiacomo.minak@unibo.it
* Correspondence: cbx086@coventry.ac.uk

Abstract

Despite increased utilization of high-performance mortars in construction, there remains a paucity of research concerning the bond performance of steel reinforcement, particularly within masonry structures. This study characterizes the bond stress behavior in high-performance steel fiber mortar (HPSFRM) to define critical design bond stress parameters. Pull-out tests were performed, incorporating three primary variables: compressive resistance, steel fiber volume, and steel rebars diameter. To support safe and reliable bond design in HPSFRM precast members, various methods for analyzing bond strength, alongside empirical predictive equations, were evaluated. The results revealed that although the rate of increase in bond strength was impacted by the incorporation of steel fibers, the bond strength demonstrated significant improvement in the mortar compressive strength. Introducing steel fibers at a volumetric content of 1% doubled the bond strength. The optimum fiber content was found at 1%, where bond strength increased by 6% and slip by 102% due to effective fiber bridging. Increasing the dosage to 2% yielded only a marginal 2–5% gain, hindered by clustering and poor dispersion. Variations in steel bar diameter had a more pronounced effect on bond stress behavior. The proposed model addresses the underestimation of bond strength and ductility by existing empirical models and code provisions.

Keywords: bond behavior; high-performance; masonry; steel fiber; pull out

Academic Editor: Catalin R. Picu

Received: 26 October 2025
Revised: 23 November 2025
Accepted: 1 December 2025
Published: 5 December 2025

Citation: Amrouche, R.S.; Djaknoun, S.; Saidani, M.; Abeoub, Z.; Minak, G. Bond Stress Analysis Between High-Performance Steel Fiber Reinforced Mortar and Deformed Steel Bars Under Pull-Out Test. *Fibers* **2025**, *13*, 164. https://doi.org/10.3390/fib13120164

1. Introduction

Over the last three decades, new materials have been developed for construction projects to enhance the ductility of high-performance concrete and mitigate the risk of brittle failure under tensile and compressive loading conditions. Recommendations for the use of ultra-high-strength and high-strength concrete have been proposed [1,2]. Nonetheless, the current codes are still based on the design principles established for plain concrete. The formulation has been developing high-performance and ultra-high-performance mortar (HPM) in France [3]. Mortar is classified as a material capable of achieving uniaxial compressive strengths of 105 MPa or greater. High-performance mortar (HPM) is designed to achieve a dense matrix and exhibit superior compressive strength, typically exceeding 100 MPa. This study examines the bond performance of ribbed steel rebars embedded

within a high-performance mortar matrix reinforced with steel fibers, particularly when applied to masonry substrates, as the existing literature on this subject remains limited. High-performance cement mortars reinforced with steel fibers are increasingly used in surface coatings or in bed joints of masonry walls to enhance tensile resistance and structural integrity. They are also incorporated into the mortar bed joints of masonry structures [4]. An overview of these applications is shown in Figure 1. The exclusion of coarse aggregates contributes to reduced ductility and brittle failure under both compression and tension [5]. The exclusion of coarse aggregates in high-performance mortar (HPM) results in a finer and more homogeneous matrix; however, this comes at the expense of ductility, markedly influencing its mechanical behavior under both tensile and compressive loading. In the absence of coarse aggregates, the mortar lacks the crack-arresting mechanisms and interfacial transition zones (ITZs) that, in conventional concrete, contribute to energy dissipation, thereby promoting a more brittle failure mode [6,7]. Under tensile loading, HPM generally fails through the formation of a single, localized crack with limited deformation, in contrast to concrete, which exhibits distributed microcracking due to aggregate interlock and crack deflection [8]. Under compressive loading, the absence of coarse aggregates eliminates their function in impeding crack propagation, leading to abrupt, explosive failure with reduced post-peak ductility, as opposed to the more progressive, multi-cracking failure observed in conventional concrete [9]. To mitigate these limitations, HPM formulations frequently incorporate fibers (e.g., steel, polyvinyl alcohol, or polypropylene) to enhance tensile strain capacity, as well as supplementary cementitious materials (SCMs), such as silica fume, to refine the microstructure and improve overall toughness [10]. Nonetheless, even with such modifications, mortars remain intrinsically less ductile than conventional concrete. In the present study, the optimized water-to-cement ratio enhanced the matrix strength, while the inclusion of steel fibers improved ductility and contributed to a more favorable failure response. High-Performance Steel Fiber Reinforced Mortar (HPSFRM) is a sophisticated, strain-hardening cementitious composite (SHCC). It is formulated by precisely combining cementitious materials, fine aggregates, water, and discontinuous steel fibers, often with various chemical additives. The material's design is guided by the principles of fine mechanics and fracture mechanics, specifically optimizing the role of fiber bridging across developing microcracks. Consequently, HPSFRM successfully overcomes the inherent brittleness of ordinary concrete. This advanced composition results in superior mechanical properties, including significant strain-hardening behavior under direct tensile loading and exceptionally high toughness and ductility when subjected to compressive forces. This material significantly enhances the structural ductility. It exhibits key characteristics such as crack arrest and increased density, resulting in positive application effects in both structural reinforcement and seismic resistance.

The increasing adoption of steel fiber-reinforced concrete (SFRC) is due to its superior mechanical characteristics relative to traditional plain concrete [11]. Steel fibers are commonly incorporated into HPM and UHPM. Characterized by steel fiber reinforcement, this material is considered a high-performance mortar. HPSFRM tends to exhibit a low water-cement ratio. Ensuring the reliable and efficient use of HPSFRM as precast members in civil infrastructure requires extensive knowledge of the bonding characteristics of the involved materials. Splitting tensile and compressive strength are key factors affecting the bond between mortar and conventional reinforcement, and the Fraction volume of different kinds of fibers also covers mortar. The transfer of bond stress between ribbed rebars and mortar encompasses three fundamental parts: the bond mechanisms include chemical adhesion, friction resistance, and mechanical interlock between the steel ribs and the encasing mortar [12]. The following phenomena are often associated with bond failure of bars [13]: The mortar experienced local failure directly ahead of the reinforcement ribs,

and/or the mortar surrounding the steel bars splits when the radial stress causes it to split, resulting in splitting failure. Localized crushing of the mortar ahead of the ribbed reinforcement under high radial stresses occurs more frequently when there is significant confinement from either the surrounding mortar or transverse reinforcement, or when the rib height is relatively small. When confinement is insufficient and the rib height of the reinforcement is substantial, radial stresses lead to longitudinal cracking and mortar splitting, making it the dominant bond failure mechanism, resulting in a mechanism that tends to exhibit brittleness.

Numerous studies have explored the significance of incorporating steel fibers into cementitious matrices to enhance the bond stress behavior between mortar and ribbed steel reinforcement. The addition of steel fibers is well-established to improve the overall mechanical characteristics of concrete and mortar, notably enhancing their ductility, tensile strength, and resistance to crack development [14–16]. These improvements are highly beneficial for the bond performance; researchers have indicated that the fibers act as internal confinement, which reduces splitting tendencies and thereby enhances the adhesion between concrete and ribbed steel reinforcement bars [17,18]. Beyond improving bond strength and crack mitigation, steel fiber-reinforced mortar (SFRM) and concrete (FRC) have been demonstrated to effectively increase the energy absorption and damping capacity of structures, making them particularly advantageous for seismic and shock-resistant applications [17,19]. Due to this combination of enhanced mechanical behavior, bond performance, and durability, steel fiber-reinforced composites are gaining increasing popularity in specific, high-performance applications [14]. Recent studies have shown that bond strength increases with fiber volumetric proportion (up to 3%), as well as with bar diameter [20], The incorporation of steel fibers into UHPC led to noticeable changes in bond behavior compared with fiber-free mixes. At a fiber content of 1%, bond strength increased by about 6%, while the corresponding slip rose sharply by 102%. These enhancements are mainly linked to the fiber-bridging mechanism, which improves the tensile resistance of the matrix and delays the onset of splitting. Beyond this dosage, however, the gains in bond strength were marginal. The highest average bond strength recorded was 61.49 MPa at 3% fiber volume, only 0.2% higher than the value obtained with 1% fibers. At greater fiber dosages, bond strength showed a slight decline, although the free-end slip at peak load continued to rise gradually up to 5%, following a trend different from that of bond strength [20]. Other researchers, such as [21], investigated four fiber dosages (1%, 2%, 3%, and 4%) and obtained compressive strengths of 197, 202, 207, and 185 MPa, respectively. These results indicate that while the incorporation of steel fibers enhances compressive strength, the rate of improvement decreases as the fiber volume fraction increases. At higher dosages, the reduction in performance can be attributed to fiber clustering and poor dispersion within the cementitious matrix. With respect to bond behavior, all specimens failed by pullout rather than splitting, as the splitting tensile strength of the UHPFRC surrounding the rebar was greater than the radial component of the bond stress. For UHPFRC mixtures without coarse aggregate, bond strength generally increased with fiber addition; however, the rate of increase diminished beyond 1% fiber content. Other scholars [21] reported similar findings, noting that while steel fibers improve the bond strength of deformed steel bars in SF-RPC, the enhancement becomes marginal once the fiber content exceeds 1%. For example, at 2% fiber content, the gain in bond stress was limited to only 2–5% compared with 1%. This behavior highlights the importance of fiber dispersion in achieving effective stress transfer. Moreover, the choice of limiting fiber content to 1% in the present work is supported by the characteristics of the hooked-end fibers employed (50 mm in length), which tend to exacerbate dispersion issues at higher dosages. Consistent with earlier studies [5], steel fibers were found to substantially increase bond strength by more

than twice that of plain UHPC, but the incremental benefits decreased with additional fiber content, and no significant improvement in splitting bond strength was observed beyond 1%.

The thickness of the protective concrete cover exerts a substantial influence on the bond failure mechanism. It has been reported that steel fibers can more than double the bond strength of UHPC Relative to UHPC without steel fibers [22]. Nevertheless, with the rise in the volumetric fraction of fibers, the rate of improvement declines, and beyond 1%, no substantial improvement in splitting bond strength can be anticipated. The failure behavior of Ultra-High-Performance Concrete (UHPC), Steel Fiber-Reinforced Concrete (SFRC), and High-Performance Steel Fiber-Reinforced Mortar (HPSFRM) under pull-out loading reveals a key commonality: the transition between failure modes is governed by the embedded length of the reinforcing bar. For UHPC and SFRC, a pull-out failure is prevalent when the embedded length is less than 5 times the bar diameter (5d), a behavior also influenced by the concrete cover. When the embedded length exceeds 5d, all three materials exhibit a splitting failure mode [21]. In HPSFRM, this is specifically characterized by the exceedance of the mortar's tensile stress capacity [4]. However, their bond stress-slip behaviors diverge significantly. In HPSFRM, the response leading to tensile splitting is predominantly linear with slight non-linearity before failure, and a post-peak response is often absent due to the material's brittle nature [4,23,24]. Conversely, the bond stress in UHPC and SFRC is derived from chemical adhesion, friction, and mechanical interlock. The chemical adhesion diminishes rapidly under load for deformed bars, leaving mechanical interlock as the primary resistance mechanism, with a non-uniform stress distribution along the bar length. Frictional forces only contribute significantly upon the initiation of slip between the bar and the concrete [14]. In the literature review, these distinctions were addressed by highlighting the influence of matrix densification, the absence of coarse aggregates, and the crack-bridging role of fibers. Moreover, the review highlights the differences in peak bond stress, failure modes, and post-peak softening between UHPC and conventional SFRC, while also noting the limited applicability of conventional bond models and the need for UHPC- and HPSFRM-specific formulations [25].

The impact of steel fibers on bond performance behavior between high-tensile-strength concrete and glass or polymer fiber-reinforced or ribbed steel rebars has been investigated, emphasizing their role in improving bond strength and overall structural integrity [26]. Researchers have observed that steel fibers enhanced the bond behavior between concrete and ribbed rebars by margins ranging from 5% to 70%. The most significant improvement was observed with a steel fiber dosage of 40 kg/m^3. The impact of high temperatures on the bond stress in fiber-reinforced concrete has been investigated, revealing its influence on bond strength and overall structural performance [27]. It was found that concretes containing 2% steel fibers by volume exhibited a 23% increase in bond performance compared to plain concrete. Furthermore, the study revealed that the steel fibers had a positive influence on the bond strength when exposed to high temperatures. Most UHPC mixtures eliminate coarse aggregate and utilize fine aggregate (FA) typically smaller than 0.6 mm to reduce the interfacial transition zone ITZ and improve the uniformity of the mixture [28,29]. Bond stress can be impacted via multiple factors, such as increased fiber volume fraction and bond stress, and slip at peak pull-out load, mainly as a result of improved compressive strength [28]. An enhancement of the fiber volume fraction has contributed to the enhancement of bond stress and the amplification of slip at peak load, reaching optimal enhancement at up to 2%. This enhancement is mainly due to the reinforcing action of the fibers, which enhances the material's overall mechanical performance [14]. Bond strength has been shown to increase with larger bar diameters [11]. Nevertheless, research examining the interfacial bond behavior between HPSFRM and ribbed reinforcement remains

relatively limited. Moreover, a bond stress-slip model for HPSFRM with steel reinforcement has yet to be developed and remains an urgent research need. The estimation of ultimate splitting bond stress between reinforcement and concrete has been approached through different formulations, with numerous researchers proposing empirical expressions. Design codes also provide equations, but most do not distinguish the governing failure mechanisms. Among them, the ACI design code [29] is one of the few that explicitly incorporates the influence of the failure pattern. The equations examined in this study indicate that the most critical parameters affecting bond stress are the compressive strength of the concrete and the ratio of cover thickness to bar diameter. Embedment length is also considered, as the distribution of stresses along the bar influences the average bond resistance. Code provisions generally address this through development length equations, reflecting the effect of stress states caused by bending or direct tension [5]. Other empirical formulations further account for factors such as bar size, placement, and location within the section. Nevertheless, no existing analytical models describing either the peak bond strength or the full bond stress–slip response have been validated for steel bars embedded in HPSFRM. There are alternative materials that advance the ductility of HPC and decrease the risk of brittle failure subjected to tensile and compressive loading conditions loading such as this study [30], which gives a foundational understanding of the interfacial bond behavior is paramount for the reliable application of advanced cementitious composites, particularly in structural repair. For instance, recent investigations into repair systems using Carbon Fabric Reinforced Cementitious Matrix (CFRCM) composites have relied on pull-out testing and rigorous modeling to characterize the critical fabric-matrix bond. A recent investigation showed that ICCP significantly reduces the tensile strength and ultimate strain of CFRCM in corroded RC beams as charge density increases. An improved piecewise tensile constitutive model was developed to better predict the polarized material's behavior. This highlights the importance of accurately characterizing strengthening materials under environmental stress, aligning with the focus on bond stress analysis [31,32]. For better engineering application of HPSFRM, this study [33,34] shows that UHPFRC jackets significantly improve the axial capacity of corrosion-damaged RC columns and markedly slow corrosion progression. Enhanced structural performance depends strongly on the bond quality between UHPFRC and the existing concrete and steel surfaces. Overall, the findings highlight the vital role of a durable interface for effective load transfer and long-term protection in retrofitted columns.

Therefore, comparisons between experimental findings and conventional empirical or code-based equations may not reliably capture the bond behavior in HPSFRM systems.

This study presents a comprehensive experimental investigation into the bond performance of ribbed steel reinforcement bars anchored in high-performance steel fiber-reinforced mortar (HPSFRM), utilizing a standardized pull-out test configuration. The primary objective is to quantitatively assess the influence of two critical parameters: the compressive strength of the HPSFRM matrix and the diameter of the ribbed steel bar. Currently, the field is hindered by a significant lack of experimental data, which has precluded the development of a robust bond stress-slip constitutive model specifically for HPSFRM. This research directly addresses this gap by generating a reliable dataset to facilitate the creation of such a model. Furthermore, the efficacy of existing code provisions and empirical formulas for estimating bond strength in plain concrete and UHPC will be rigorously evaluated against experimental results to determine their applicability and limitations for this advanced material, thereby establishing a vital foundation for the future development of targeted design guidelines for HPSFRM structures.

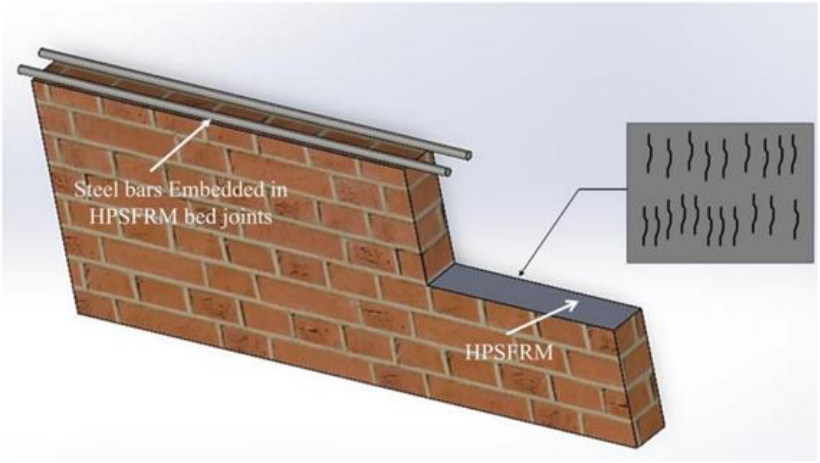

Figure 1. Use steel-reinforced cement high-performance steel fiber mortar in masonry walls.

2. Materials and Methods

2.1. Materials

The mortar material was designed based on a typical composition used in a previous study [3]. The concretes examined were produced using mixed designs incorporating standardized sand. Accordingly, the mixtures consist of standardized sand, CEM I 52.5 R high-strength cement, silica fume, superplasticizer, accompanied by faucet water, with no steel fibers included. The mix was modified by incorporating 1% steel fiber into the other mortar mix.

2.2. Steel Fibers

To enhance the characteristic performance of High-Performance Steel Fiber Reinforced Mortar, steel fibers were introduced into the mix, with particular emphasis on the improvement of its tensile strength and toughness [32]. Hooked-end steel fibers, marketed under the trade name Dramix (Petrovice u Karviné, Czech Republic), specifically the 3D 55/30 type, with a length of 30 mm. The geometric characteristics of the steel fibers are illustrated in Figure 2. A comprehensive overview of the characteristics of the steel fibers used is shown in Table 1. The fiber volume fractions varied between 0% and 1%.

Figure 2. Hooked-end steel fibers were used in the study.

Table 1. Steel fiber performance characteristics.

Type of Fiber	Diameter (mm)	Length (mm)	Length-to-Width Ratio (lf/df)	Wire Ductility (%)	Tensile Strength (MPa)	Elastic Modulus (GPa)
Hooked end	1.05	50	47.62	0.8	1115	200

2.3. Cement and Standard Sand

Within the scope of this study, high-strength CEM I 52.5 R Portland cement, fabricated by LAFARGE following NF EN 197-1 [35], was used. It has a relative density of 3.156 g/cm^3 and a Blaine fineness of 326 m^2/kg [36]. Table 2 presents the physical properties and chemical compositions of both the cement and silica fume. The standard sand was obtained from SNL in France, as can be seen in Figure 3, and was certified by EN 196-1 [37]. The fine particles of silica fume used were from Sika (Baar, Switzerland) (Eucalyptus, Algeria). Table 3 furnishes the physical characteristics and sieve analysis of the aggregates. A liquid super-plasticizer, fabricated by Ska, containing polycarboxylate, was used. It is a range-reducing admixture complying with the standard NF EN 934-2 [38].

Figure 3. Sand grading conforming to EN 196-1 standard [37].

Table 2. Portland cement and silica fume: Compositional chemistry and physical characteristics.

Chemical Analysis (%)	Portland Cement	Silica Fume
SiO_2	20.09	85
CaO	64.02	1.00
SO_3	2.83	2.0
Fe_2O_3	3.87	-
Al_2O_3	4.84	-
MgO	1.15	-
Na_20	-	1.0
Si	-	0.4
Cl-	-	0.1
Physical analysis (%)		
Loss On Ignition	2.36	-
Specific Gravity	3.156	-
Fineness (m^2/g)	0.326	Between 15–35

Table 3. Granulometric Distribution and Physical Characteristics of Standardized Sand.

Sieve Size (mm)	Cumulative Refusal (%)
2	0
1.60	7
1	33
0.5	67
0.16	87
0.08	99

2.4. Reinforcement Steel

Nominally 10 mm and 12 mm diameter ribbed steel rebars were selected for use in the experimental program. Laboratory measurements of the high-strength hot-rolled ribbed steel rebar indicated a yield stress $\mathbf{f_y}$ of 520 MPa and an ultimate tensile strength $\mathbf{f_u}$ of 606 MPa. These bar diameters are widely used in civil engineering applications. The bars featured a crescent-shaped surface deformation pattern, comprising two longitudinal ribs linked by circular transverse ribs orthogonal to the steel rebar baseline, as illustrated in Figure 4.

Figure 4. Surface deformation of steel bars.

2.5. Mortar Mix Proportion (Preparation, Mixing, and Curing)

An overview of the HPSFRM mix proportions employed in the current research is detailed in Table 4. The proportion of water relative to binder (W/B) ratio of 0.25 was used for each of the test specimens. The mixing process was tightly controlled to ensure uniformity between batches and effective fiber dispersion. All mixing was conducted using a laboratory-scale vertical-axial mixer with a 65 L capacity, following a precise sequence with strict timings:

- Dry Mixing of Solids: Fine aggregates were incorporated into the mixer and mixed at a low speed for 2 min to ensure a uniform base.
- Addition of Binders: Cement and silica fume were then added on top of the fine aggregates. Dry mixing continued at a medium speed for 2 min to achieve a homogenous distribution of all solid constituents.
- Addition of Liquids and Fibers: The liquid component, a pre-mixed blend of water, superplasticizer, and the requisite amount of steel fibers, was introduced gradually over half a minute while the mixer operated at a low speed to prevent fiber balling.
- Wet Mixing: After all components were added, the wet mixture was mixed at a high speed for 2 min to ensure complete coating of the aggregates and uniform fiber distribution throughout the mortar matrix.

No resting periods were introduced between stages. This procedure, resulting in a total mixing time of 6 and a half minutes, was consistently followed for all HPSFRM batches and was designed based on established methodologies from previous studies [39].

In concrete and mortar mix design, the superplasticizer dosage is conventionally defined as the mass percentage of its active solid content relative to the total mass of the dry binder. For the mix in Table 4, the total binder mass is 495 kg, comprising 450 kg of cement and 45 kg of silica fume.

Since commercial superplasticizers are aqueous solutions typically containing 30–40% solid content, the mass of the liquid admixture used must be converted to its equivalent dry mass of active solids. Consequently, the specified dosage of 1.5% refers to the proportion of dry superplasticizer solids relative to the total dry binder mass.

As mentioned above, all specimens were prepared with a fixed ratio (W/C) of 0.25. This choice follows the continuity of the doctoral research conducted by [40], who carried out extensive investigations on two high-performance concrete formulations based on standardized sand. The work, focused on the mechanical behavior and durability of concrete at elevated temperatures, included three-point bending tests on notched specimens. The results demonstrated that, for unheated mortars, the incorporation of silica fume combined with a W/C ratio of 0.25 led to a significant enhancement of mechanical strength: approximately +50% in tensile strength and +30% in compressive strength. Furthermore, the addition of silica fume resulted in a notable reduction in porosity (−14.8%), and a 10% replacement with silica fume decreased porosity by nearly 48%. These findings were accompanied by changes in pore structure, with a considerable increase in the proportion of micropores, which accounted for almost the entirety of the measured porosity. In particular, it was observed that between ambient temperature (25 °C) and 300 °C, the failure load increased. This phenomenon was attributed to the continued and accelerated hydration of cement, which strengthened the bonds between the mortar constituents. Similarly, ref. [3] adopted the same formulation (W/C = 0.25) within an experimental and numerical framework to analyze the mechanisms of thermal degradation in mortars.

To maintain the workability of the concrete matrix, which is typically reduced by the addition of steel fibers and a low water-to-binder (w/b) ratio, a superplasticizer was incorporated [5]. In that study [5], three different water-to-cement ratios were tested (0.25, 0.20, and 0.17). The results demonstrated that compressive strength increased as the w/c ratio decreased, reaching approximately 100, 150, and 200 MPa, respectively. This confirms that the w/c ratio is a key factor influencing the matrix strength. Furthermore, the same study [5] indicated that workability can be improved by using smaller-diameter steel fibers rather than longer ones. In concretes with a very low w/b ratio, the use of hooked-end fibers tends to promote fiber balling, which significantly reduces workability. To avoid this effect, the present study employed short, straight steel fibers. Finally, it was found that increasing the compressive strength of the concrete led to a proportional rise in the ultimate bond stress, while the volume of steel fibers had only a limited effect. To achieve the desired flowability of the HPSFRC, a polycarboxylate-based superplasticizer (SP) was introduced as a high-efficiency water-reducing admixture [30].

The experimental program was structured to isolate the influence of matrix compressive strength, fiber volume ratio, and rebar diameter by adopting a controlled, factorial-type design. First, the mix compositions were proportioned to vary only the target compressive strength while keeping other parameters, such as water-to-binder ratio and curing regime, constant. Second, the fiber content was systematically adjusted across predefined volume ratios, with all other mix proportions unchanged to avoid interaction effects with matrix strength. Third, different rebar diameters were tested under identical embedment length and cover conditions, ensuring that other parameters did not confound the effect of bar

size. Each parameter was therefore modified independently while the others were held constant, and specimens were cast and cured under uniform conditions to minimize variability. This approach allowed the experimental results to be attributed directly to the three main variables of interest, thereby reducing confounding influences and enabling clearer interpretation of their individual and combined effects on bond behavior.

Table 4. Quantities of materials for producing 1 m^3 of mortar, specified in kg/m^3.

Steel Fiber	W/C Ratio	Cement	Water	Sand	Silica Fume	Superplasticizer
0.Vol% 1.Vol%	0.25	450	112.5	1350	45	6.5

Note: V_f = volume fraction of fiber.

3. Pull-Out Test Setup

3.1. Preparation of Specimens

The bond response of ribbed steel rebars in high-performance steel fiber reinforced mortar (HPSFRM) was evaluated through pull-out tests conducted following the RILEM RC6 Strategic guidance, RILEM TC 1994 [41]. The preparation of 100 mm cubic samples followed the method depicted in Figure 5. Each sample incorporated one bar positioned precisely along its central longitudinal axis. The cleaning process must not modify the bar's surface roughness. The bar should be entirely free of rust and, if needed, may be degreased with carbon tetrachloride (CCl_4) or ethylene trichloride (C_2HCl_3). When the test bar is corroded, according to the RILEM RC6 Strategic guidance, RILEM TC 1994 [41].

The rebar bond length was established to be five times the rebar diameter and embedded at the bottom of the mortar cube, following the guidelines specified by RILEM RC6 [26]. To clarify the rationale for selecting an anchorage length of five times the bar diameter (5d), this choice is consistent with recommendations in international guidelines such as RILEM RC6 1994 [41], which suggest 5d as an effective embedment length to achieve a representative bond failure mechanism while avoiding premature failure at the loading interface. More recent studies [4,14] also confirm that this criterion provides a suitable balance between mobilizing the full bond capacity and limiting bar-end or localized crushing effects. Moreover, for specimens with bar diameters of 10 mm and 12 mm, mortar splitting failure was observed, which commonly occurred when the anchorage length exceeded 5d, regardless of the mortar type used [4]. The bond length was located as far as possible from the loading end to reduce parasitic compressive stresses along the bonded zone and to avoid cone-shaped failure at the loaded surface [32]. The pull-out test specimen is indicated in Figure 5b.

The unbonded portion of the reinforcement bars was wrapped with plastic tape before placement in the mortar. This was performed to precisely define the bond length, prevent contact between the rebar and mortar outside the bonded zone, and inhibit the penetration of cement paste into the unbonded areas. In this context, the bonded and unbonded region lengths are denoted by l and l_{un}, respectively. Following the casting of the mortar, Plastic sheeting was used to envelop the surfaces of the specimens. To confirm that the bond behavior between the ribbed rebars and mortar aligns with the requirements of the intended application, all samples were cured for 24 h in a laboratory environment maintained at 22 °C with a relative humidity of 55–75% before demolding. As depicted in Figure 6, following storage in a curing tank, at 28 days, both mixing and curing utilized tap water. All curing procedures were conducted in compliance with the NF EN 12390-1 standard [42].

(**a**)

(**b**)

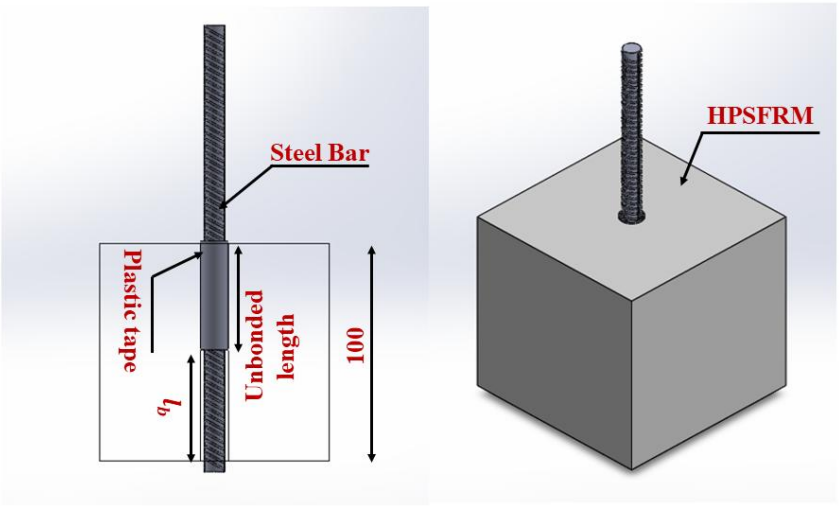

Figure 5. Molds prepared with embedded rebars for pull-out testing, illustrating the: (**a**) specimen configuration adopted in the experimental program. (**b**) Cube specimen details (unit: mm).

Figure 6. Specimens in the tanks.

3.2. Test Setup and Instrumentation

A universal materials testing apparatus (MTS, Eden Prairie, MN, USA), was employed to conduct the tests with a 300 kN capacity in uniaxial tension, enabling displacement-controlled tests. The testing machine and experimental setup are illustrated in the photograph in Figure 7. The support comprises a steel plate anchored to the hard floor via a supporting structure. The mortar cube was positioned in abutment with the steel plate used in the assembly, which featured an Axial hole with a diameter equal to twice that of the steel bar, allowing the rebar (loaded end) to pass through. The test setup and support conditions were established following RILEM RC6 [41], as illustrated in Figure 7. A 5 mm rubber support plate was positioned between the mortar samples and the steel support block to ascertain uniform pressure distribution and to prevent bending or displacement caused by surface irregularities at the contact interface during loading. A rubber pad was placed between the samples and the bearing plate to reduce the compressive force generated at the interface throughout the pull-out test. The bar was loaded at a constant rate of 0.02 mm/s. Accordingly, displacement control mode was employed for all testing procedures to accurately capture the post-peak behavior, with the applied load quantified by the machine's electronic load cell. An extensometer integrated into the MTS testing machine was used to record the displacement of the rebar during pull-out loading. This setup allowed precise monitoring of slip development at the steel–mortar interface.

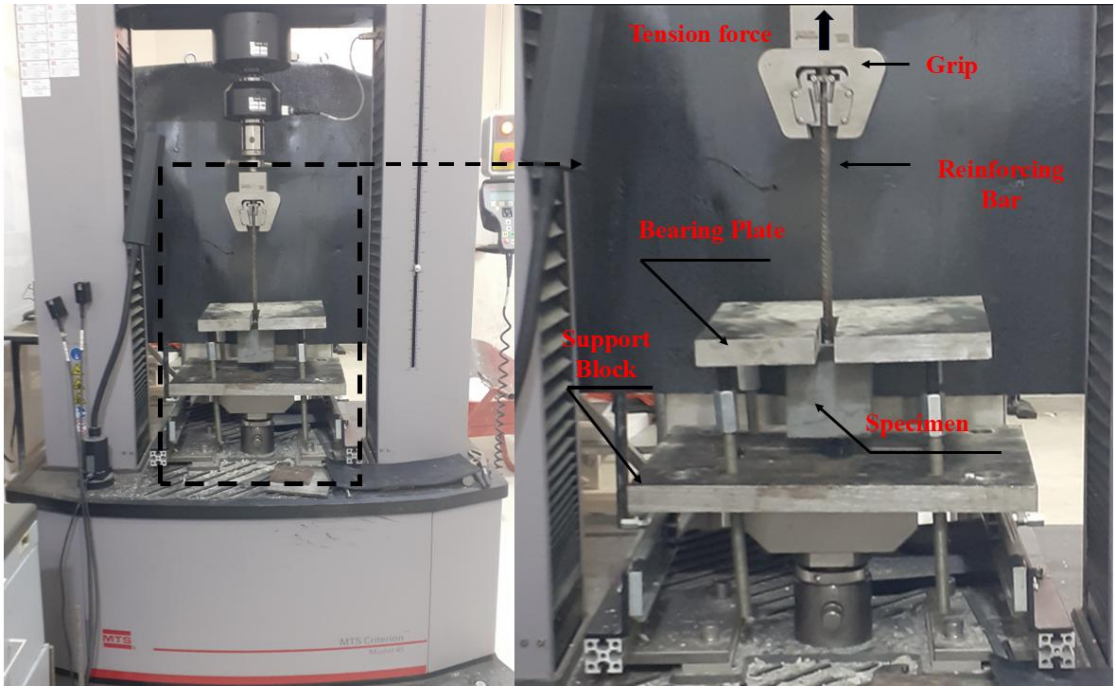

Figure 7. Pull-out test setup in the MTS machine, illustrating the specimen configuration and loading arrangement.

3.3. Materials Test

HPSFRM compressive strength specimens were fabricated concurrently with the pull-out samples and subjected to uniform parameters of curing conditions until testing. To measure compressive strength, A hydraulic-based universal testing device with a maximum capacity of 2000 KN was employed. The test setup is presented in detail in Figure 8. A constant load velocity of 0.6 ± 0.2 MPa/s was evaluated following the NF EN 12390-1 standard [42], and the load was incrementally maintained until structural failure ensued. An overview of the results is presented in Table 5. Each result presented is the average

of three independent sample measurements, ensuring a more reliable and representative measurement by minimizing variability and enhancing the robustness of the data [20].

Figure 8. Sample in the compression testing machine.

Table 5. Outcome of the pull-out test.

Type	P^{α}_{max}(KN)	SD	s^{α}_{max}(mm)	SD	τ^{a}_{u}(Mpa)	SD	$\tau^{a}_{R}=\frac{\tau^{a}_{u}}{\sqrt{f_{cu}}}$	SD	Failure Modes	f_{cu}(MPa)	SD
HPSFRM-0-10	43.373	±1.85	6.73	±0.41	25.98	±1.11	3.15	±0.19	SP	68	± 1.5
HPSFRM-1-10	44.457	±0.38	6.43	±1.26	26.21	±0.66	3.08	±0.17	C	72	± 2.1
HPSFRM-0-12	43.539	±2.74	3.76	±0.29	13.8	±0.87	1.67	±0.13	SP	68	± 1.5
HPSFRM-1-12	47.338	±1.95	5.64	±0.53	19.12	±0.79	2.25	±0.21	C	72	± 2.1

Note: f_{cu}—Compressive strength; P^{α}_{max}—Average Peak load; s^{α}_{max}—Typical slip corresponding to peak load; τ^{a}_{u}—bond strength average; τ^{a}_{R}—nominalized bond strength average; SD is Standard deviation; SP is splitting failure; C is Combined Failure (A combination of pull-out and subsequent splitting failure).

4. Experimental Results and Discussion

To assess the bonding interaction of ribbed steel bars in high-performance steel fiber-reinforced mortar, the results of the cube tests were utilized. Using the failure load obtained from the pull-out procedure, the bond strength was computed via division of this load by the surface area of the rebar's bonded length, as defined by Equation (1):

$$\tau = \frac{F}{\pi\, d_b l_b} \quad (1)$$

where τ—bond strength, F—failure load, d—Steel reinforcement diameter, and l_b—Anchorage length of the reinforcing bar.

To examine the bond strength characteristics of HPSFRM in comparison with and without steel fibers, the effect of varying compressive strength was formally recognized. The bond strength is standardized by dividing it by $\sqrt{f_{cu}}$, per a widely adopted approach in the literature [41], Equation (2) is shown below.

$$\tau_R = \tau_u / \sqrt{f_{cu}} \quad (2)$$

where τ_R stands for the standardized bond stress and f_{cu} indicates the compressive strength of the mortar. Table 5 displays the results.

4.1. Results

Table 5 shows that reduced rebar diameters are linked with higher average bond strengths and the corresponding slips. For diameters of 10 mm and 12 mm, the bond stresses are 25.98 MPa and 13.8 MPa, respectively, for a 0% fiber content, and 26.21 MPa and 19.12 MPa for a 1% fiber content. Table 5 summarizes the experimental outcomes of the pull-out tests performed on ribbed steel bars embedded in high-performance steel fiber-reinforced mortar. For each specimen type, the table reports the average peak load (P^{α}_{max}), the slip corresponding to this peak load (s^{α}_{max}), and the ultimate bond strength (τ^{a}_{u}). To allow comparison between specimens with different mortar strengths, a normalized bond strength ratio (τ^{a}_{R}) is also presented. The results indicate that bond performance is strongly influenced by both the fiber volume fraction and the bar diameter. For example, specimens with 1% fiber content (HPSFRM-1-10 series) exhibited higher bond strength values compared to plain mixes. In contrast, specimens with larger bar diameters (12 mm) showed lower normalized bond strength due to reduced confinement. The table also lists the corresponding compressive strength of the mortar (f_{cu}), which ranged between 68 and 72 MPa. Finally, the recorded failure modes reveal two main mechanisms: splitting failure (SP), characterized by radial cracks in the mortar, and combined failure (C), which involves an initial pull-out followed by splitting.

The statistical analysis of pull-out behavior, presented through robust mean $\pm$ standard deviation metrics, provides conclusive evidence that a 1% volumetric addition of steel fibers fundamentally alters the bond-slip response of high-performance mortar. While the fibers induced a statistically significant shift in failure mode from brittle splitting (SP) to combined splitting and pull-out (C) for both bar diameters, their efficacy was most profound for the 12 mm bars, where bond strength surged by a remarkable 38.5% from 13.80 $\pm$ 0.87 MPa to 19.12 $\pm$ 0.79 MPa a testament to the fibers superior crack-bridging and confining action that neutralizes the destructive radial splitting stresses inherent to larger diameters. For example, the marginally higher variability in ultimate slip (6.43 $\pm$ 1.26 mm for HPSFRM-1-10) authentically captures the stochastic nature of fiber engagement and damage propagation. This research definitively positions steel fiber-reinforced mortar as a critical material innovation for enhancing structural integrity.

The influence of reinforcing bar diameter and steel fiber content on bond strength was examined. However, it is important to note that the following comparisons are based on a limited dataset for each specific parameter combination. Therefore, the results should be considered as preliminary observations that highlight individual values rather than established statistical trends.

- Effect of Bar Diameter: It was observed that the bond strength exhibited sensitivity to variations in the diameter of the reinforcing bar. For specimens without steel fibers (0%), the average bond strength was measured at 25.98 MPa for Ø10 mm bars, compared to 13.8 MPa for Ø12 mm bars. It can be inferred that an increase in bar diameter leads to a reduction in bond strength for high-performance mortar without steel fiber, which is consistent with the well-documented phenomenon of reduced relative rib area and higher radial stresses in larger bars. A similar preliminary pattern was observed with the addition of 1% steel fibers, where the bond strength for Ø10 mm bars was 26.21 MPa, while for Ø12 mm bars it was 19.12 MPa. The presence of fibers appeared to mitigate the effect on this diameter-dependent reduction.
- Effect of Fiber Content: The addition of steel fibers also showed a preliminary correlation with bond performance. For Ø10 mm bars, increasing the fiber content from 0%

to 1% resulted in an increase in average bond strength from 25.98 MPa to 26.21 MPa. For Ø12 mm bars, a similar increase from 0% to 1% fiber content changed the bond strength from 13.8 MPa to 19.12 MPa. This indicates that the mechanical interlocking and crack-bridging action of steel fibers likely contributed to an enhancement in bond performance for both bar sizes under the conditions tested.

These individual values provide a useful initial insight into the parameter interactions. However, to properly quantify these relationships and establish definitive regression models, a more extensive dataset with additional data points across a wider range of parameters is required in future research.

4.2. Discussion

4.2.1. Failure Mode

An investigation into the fiber volume content revealed that it has a significant influence on both the bond rupture mechanism and the resulting crack pattern. Bond failure could occur in two ways: Pure splitting and coupled splitting-pull-out failure mechanisms. These findings are illustrated in Figure 9. When the rebar is subjected to high loads, a significant crack often forms in the surrounding mortar, causing it to detach from the rebar. As the rebar transmits force via rib bearing, tensile stresses develop, which can lead to longitudinal splitting cracks or simultaneous splitting and pull-out failure. Due to the confinement offered by the mortar cover or additional contributing elements, Longitudinal cracks can induce splitting in the confining mortar medium, leading to a sharp drop in bond stress. Such bond failure is known as splitting failure [42]. As shown in Figure 9c, the pull-out combined failure mode developed in conjunction with crack progression, reaching the surface.

Without steel fibers, the high-performance mortar specimens had a cover of 45 mm and 44 mm. Upon reaching the ultimate load, longitudinal surface cracks appeared, leading to sudden failure. In specimens containing 1% steel fiber, bond failure occurred through a combination of splitting and pullout from the mortar. A sharp reduction in bond stress was noted in both failure modes upon splitting of the mortar cover along the ribbed steel rebar. The presence of steel fibers significantly influenced failure behavior. Due to their bridging effect, the HPSFRM maintained structural integrity even after cracking. The dispersion of steel fibers in HPSFRM played a decisive role in modifying the observed failure modes. For example, specimens with bar diameters of 10 mm and 12 mm without fibers failed predominantly by splitting. However, when a fiber volume fraction of 1% was introduced, the failure pattern changed to a combination of splitting and pull-out, without complete separation of the specimen. This behavior can be attributed to the bridging effect of the fibers, which resist crack opening and transfer tensile stresses back into the matrix, thereby preventing catastrophic splitting as seen in Figure 9d. In contrast, in specimens without fibers, wedge action along the ribs of the reinforcing bar was more dominant, as illustrated in Figure 9b. The presence of fibers counteracted this effect by bridging across cracks generated by radial stresses, effectively redistributing stresses and delaying splitting. Consequently, the failure transitioned from pure splitting to a mixed pull-out–splitting mode, in which pull-out mechanisms contributed more significantly to the overall bond behavior. Owing to this bridging action, the concrete maintained structural integrity even after visible cracking.

The experimental results further suggest that a fiber volume content of approximately 1% was sufficient to trigger this transition in failure mode. Below this level, splitting was the primary failure mechanism, while higher fiber contents enhanced the crack-bridging capacity, providing additional confinement and altering the stress redistribution process.

Nevertheless, this threshold is not fixed and may vary depending on fiber geometry, aspect ratio, dispersion quality, and the mechanical properties of the matrix.

Splitting cracks still developed, attributable to the lack of stirrups during testing, leaving the mortar cover as the only confinement mechanism. The observed cracking pattern indicates that the mortar layer was insufficiently thick to withstand internal stresses, resulting in splitting. Concrete cover plays a critical role in governing bond behavior and the resulting failure modes. Previous studies have shown that inadequate cover thickness may lead to premature splitting due to insufficient confinement of radial stresses generated around the reinforcing bar. This study [18], for instance, examined the influence of different cover dimensions but did not fully ensure cover uniformity on both sides of the bar, which may have introduced eccentricity in pull-out tests. According to ACI 408-03 [30], a concrete cover of 3.5d or less is recommended, since once this value is exceeded, pull-out failure tends to dominate rather than splitting. Experimental evidence supports this recommendation: specimens with a 1.5d cover exhibited lower maximum bond stresses and a tendency for splitting failure, whereas bond strength improved with increased cover thickness in fiber-free concretes. When the concrete cover-to-bar diameter ratio was increased to 5.2, the specimens exhibiting a high compressive strength of 100 MPa displayed a pull-out type bond–slip response. Crucially, this behavior occurred without an accompanying significant loss in bond resistance, while in specimens with compressive strength above 150 MPa, reinforcement yielding was observed [5]. Likewise, specimens with a 3.0d cover demonstrated 2.7 times higher bond stress compared to those with only 1.5d cover, further validating the direct influence of cover thickness on bond performance [5]. However, specimens with reduced cover were sometimes overestimated by predictive code provisions, raising concerns for structural safety when insufficient cover is provided.

The effect of cover thickness becomes even more pronounced with larger bar diameters. Bond strength and corresponding slip were observed to decrease for bars with diameters of 20–25 mm, as the thin cover was unable to prevent splitting, leading to splitting-type failures instead of pull-out [20]. This highlights the strong interaction between bar diameter and cover thickness in determining bond behavior. Consistent with this, when the concrete cover was set to 2d, splitting failure was the dominant mode, while specimens with 3d, 4d, and 5.75d cover exhibited pull-out failure without visible surface cracking. In these cases, the steel bar was extracted from the UHPC matrix by shearing along the transverse ribs. The experimental program reported in [5] employed cubic specimens of 200 mm with bar diameters ranging from 10 to 25 mm, further demonstrating that the relationship between cover thickness, bar size, and failure mode is critical to interpreting bond behavior.

In the present study, the relatively thin mortar cover used is acknowledged as a potential limitation, as it amplifies splitting failures by reducing the confining capacity of the surrounding matrix. This implies that the results may represent conservative estimates of bond performance compared with field-scale applications, where larger cover thicknesses typically provide greater confinement. Nonetheless, the findings remain valuable for clarifying the fundamental mechanisms of bond in UHPC, and future work should consider specimens with increased cover dimensions to better replicate real-world masonry reinforcement conditions.

The observed bond failure modes in Figure 9a,d suggest that smaller-diameter bars are more prone to pull-out failure, leading to extensive surface cracking in the surrounding mortar. Deformations in both 10 mm and 12 mm bars produced radial forces capable of initiating splitting in the HPSFRM ahead of structural failure. Steel fibers played a crucial role in preventing splitting and promoting a more stable and ductile failure mode. In the case of the two different diameters, 10 mm and 12 mm, bond failure was characterized

by pull-out behavior along with visible surface cracks. Longitudinal cracks formed near the ultimate load, with failure occurring due to bar pull-out from the HPSFRM. The predominant cause of splitting failure was attributable to the radial stress triggered via the bearing and wedging response provided by the reinforcement ribs, which substantially facilitated longitudinal splitting adjacent to the bar. This mechanism played a key role in bond failure.

The incorporation of transverse reinforcement or additional confinement would likely alter the dominant failure mode observed in this study by reducing the tendency for premature splitting failure. In the current experiments, the absence of stirrups meant that the mortar cover acted as the sole confinement mechanism. As a result, once radial stresses from the rib bearing action exceeded the tensile capacity of the mortar, longitudinal cracks propagated rapidly, leading to splitting or combined splitting-pullout failure. Previous studies have demonstrated that transverse reinforcement can effectively restrain splitting cracks and promote a pull-out-dominated failure mode, which is generally more ductile and favorable for structural applications [43,44]. By enhancing lateral confinement, the bond utilization is increased, and sudden post-peak bond stress drops are mitigated.

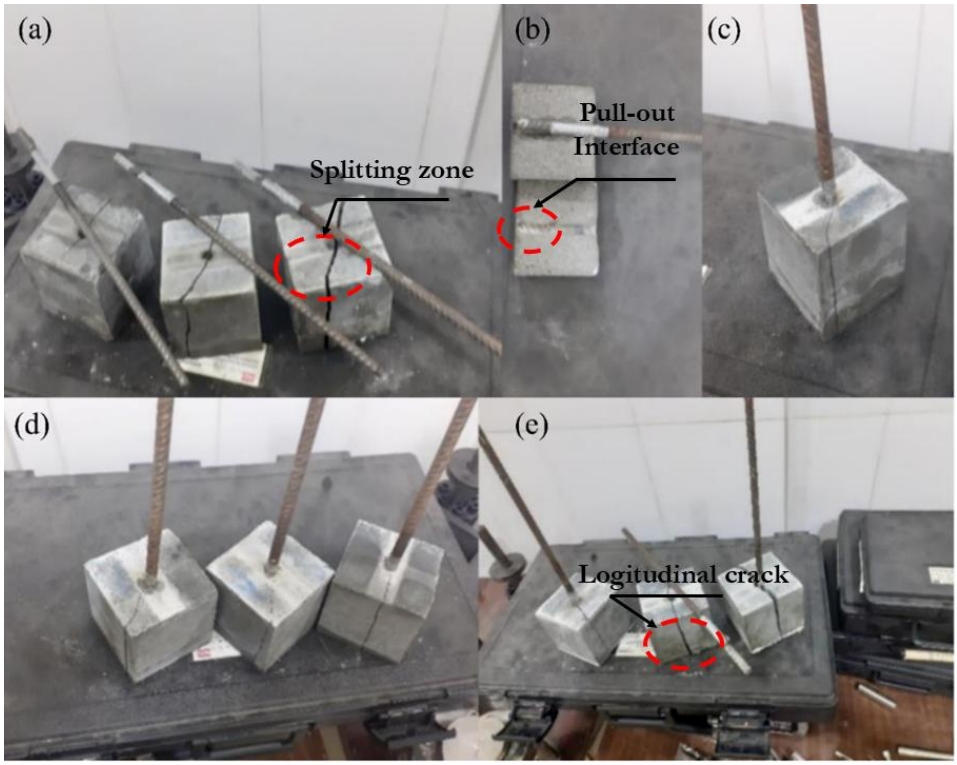

Figure 9. Failure modes: (**a**) splitting; (**b**) splitting; (**c**) integrated splitting and pull-out failure; (**d**) integrated splitting and pull-out failure; (**e**) combined splitting and pull-out.

When considered in conjunction with fiber content, confinement could further optimize bond performance. Steel fibers already contributed a bridging effect that mitigated crack opening and preserved specimen integrity after initial splitting. However, their influence alone was insufficient to prevent the initiation of longitudinal cracks in specimens with relatively thin mortar covers. Earlier research has highlighted that the combination of fibers and confinement provides synergistic effects: fibers control micro-cracking by bridging cracks, while confinement suppresses macro-crack propagation and radial expansion of the mortar cover [5,18,43]. This combined mechanism could significantly enhance both peak bond strength and post-peak ductility, thereby reducing the abrupt loss of bond stress observed in the unconfined specimens.

Furthermore, confinement would be especially beneficial for larger bar diameters, where higher radial stresses intensify the risk of splitting. Under such conditions, fibers may delay splitting, but only confinement can provide the structural restraint necessary to redistribute stresses effectively. Studies on high-strength and fiber-reinforced concretes have reported that transverse reinforcement increases the confinement ratio, delaying splitting failure and enabling pull-out mechanisms to govern bond performance [20,42]. Thus, the interaction of confinement and fiber content has the potential to produce a more stable bond stress–slip response, improving the reliability and seismic resilience of HPSFRM-reinforced masonry elements.

4.2.2. Exploring the Influence of Critical Factors on Bond Stress-Slip Characteristics, Such as Bar Diameter and Fiber Content

This section examines the relationship between rebar diameter and bond strength in steel-fiber-reinforced mortar. The behavior of the bond is significantly influenced by the mechanical interlocking effect deriving from the irregular surface topology of the ribbed steel bar, as shown in Figure 10.

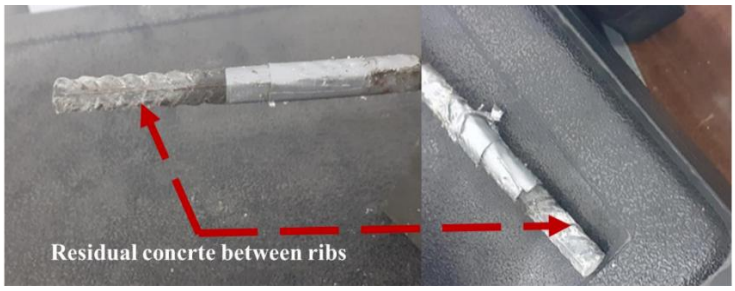

Figure 10. Morphology of bars after failure.

In Figure 11, the interaction between the ribbed steel bar and mortar is governed not solely by chemical adhesion and frictional forces.

The relationship between bar diameter and the bond performance of reinforcing bars in HPSFRM is presented in Figure 11. Results showed that smaller bar diameters achieved higher average bond strengths and corresponding slips, with strength decreasing as the diameter increased from 10 mm to 12 mm. This trend aligns with previous findings on reinforcement embedded in concrete [30,44,45]. Consequently, the use of smaller reinforcing bars is recommended to achieve higher bond strength in reinforced concrete design [20].

The observed behavior can be explained by the confinement ratio, defined as the volume of surrounding concrete relative to the bar diameter. For the 10 mm bars, the confinement ratio was 4.5, compared to 3.6 for the 12 mm bars. The higher confinement ratio provided by the smaller bars enhances the ability of the surrounding concrete matrix to restrain splitting stresses. When fibers are added, their crack-bridging and stress-transfer mechanisms act more effectively in these favorable confinement conditions, leading to a greater relative improvement in bond strength for 10 mm bars. In contrast, for 12 mm bars, the lower confinement ratio reduces the efficiency of fiber action, resulting in a less pronounced improvement. These findings indicate that fiber reinforcement is particularly effective in enhancing bond performance when smaller bar diameters are used, where confinement conditions are more favorable.

The analysis demonstrated that specimens with shorter rebar diameters sustain increased bond strength. The response curves of bond stress-slip representing the average behavior for three samples per bar diameter are exhibited in Figure 11. Initially, all samples exhibited a minor linear bond stress-slip behavior, highlighting the influence of chemical adhesion mechanisms at the interface between the deformed bars and the HPSFRM. As

microcracks formed, the bars began to slip gradually. In contrast, the ascending portion of the curve retained a linear behavior, primarily consequent upon the frictional interface mechanism between the ribbed rebar and the surrounding mortar. Before the sudden failure, the curve exhibited a small non-linear behavior. The maximum bond stress persisted across a defined slip interval until the interlocking action was compromised by the gradual deterioration of the mortar keys between the rebar ribs, leading to bond failure. The curves illustrating the bond stress-slip relationship for both rebars showed a dramatic and brutal decrease in bond stress.

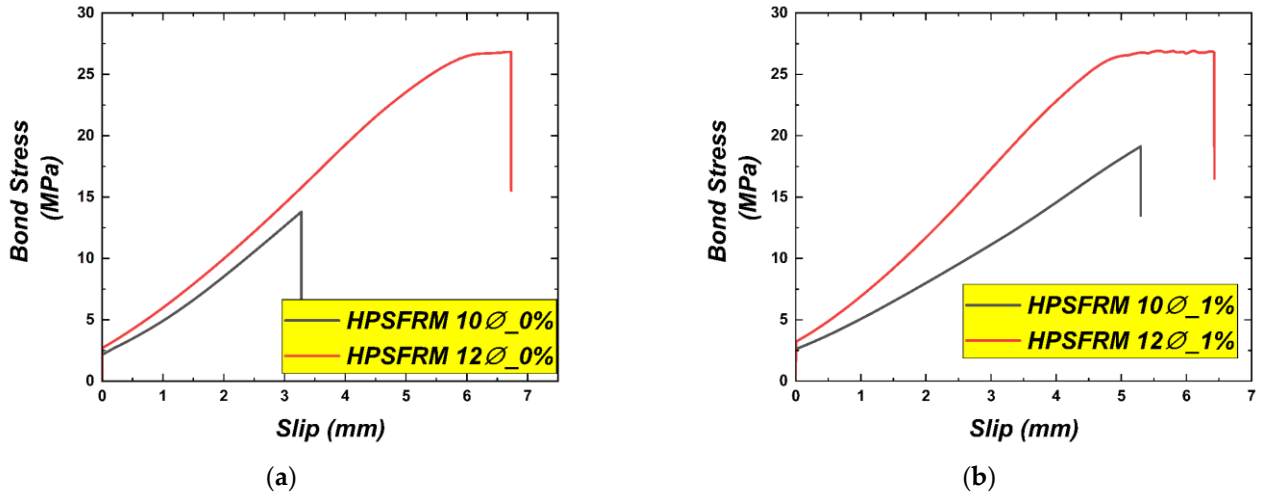

Figure 11. The specimen's bond stress versus slip behavior. (**a**) 0% fiber content, (**b**) 1% fiber content.

Two primary factors could be responsible for the diminishing bond strength associated with larger rebar diameters. The first factor is owing to the confinement effect, whereby an elevation in reinforcement steel diameter causes a decline in the confinement ratio (mortar cover relative to bar diameter), thereby decreasing bond strength [46]. The thin mortar cover used in this study was unable to prevent splitting, resulting in a splitting-type failure, as opposed to a pull-out failure. The increased thickness of the mortar covers surrounding reinforcement bars with a lesser diameter likely exerted a greater effect significantly to the bond resistance. Another contributing factor is the denser rib spacing on smaller-diameter rebars, which improves mechanical interlock, friction, and adhesion compared to larger-diameter bars [6]. Comparable findings have been presented in the existing literature for CNT-modified mortar [46] and plain concrete [47,48].

Figure 12 presents the relationship between Fiber content by volume, Mean bond strength, and the associated slip. Incorporating steel fibers into HPSFRM increased both bond strength and the associated slip when compared to the mix without fibers. Specifically, bond strength experienced a 0.89% increase, accompanied by a 4.46% rise in slip, for the bar diameter of 10 mm, and for a diameter of 12 mm, 38.55% and 50%, respectively, the observed effects of increasing fiber volume from 0% to 1% can be attributed to the fibers' bridging role, which strengthens the HPSFRM tensile capacity and prevents mortar splitting. Increasing the amount of fiber steel from 0% to 1% enhanced the Maximum bond strength for both diameters. Furthermore, in Figure 12a, there is a yielding of the bar with a 10 mm diameter, due to the internal confinement provided by the steel fiber and its small diameter. Thus, increasing the fiber content makes the HPSFRM more ductile.

Similar trends have been reported in previous research concerning fiber content in mortar. According to the conclusion of [6], by mitigating crack growth within the mortar, steel fibers contribute to increased pull-out resistance of embedded strands. Pull-out strength was enhanced by over 30% due to fiber reinforcement.

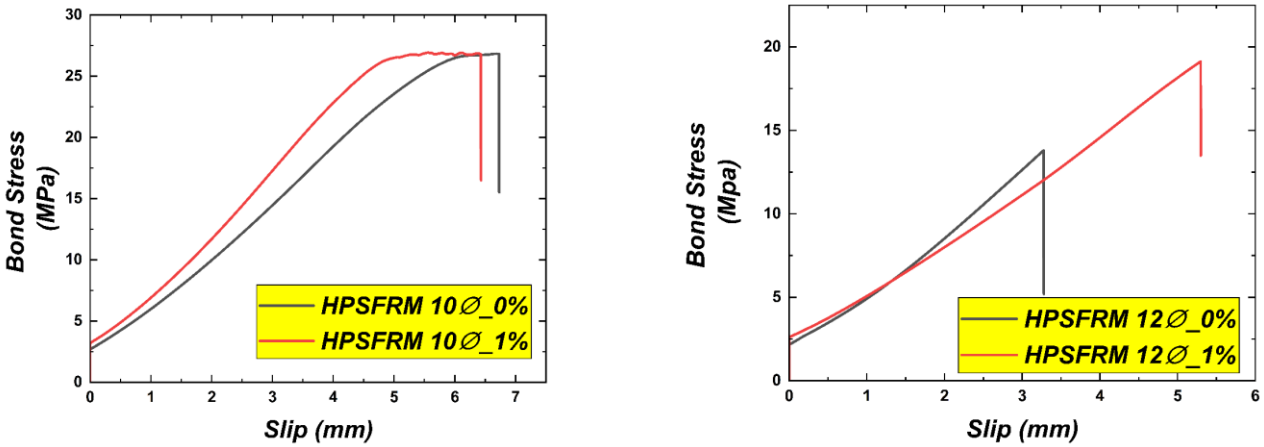

Figure 12. Bond stress-slip behavior observed in the specimen. (**a**) 10∅ steel bars, (**b**) 12∅ steelbars.

As reported in [49], an Enhancement of bond strength was observed, with a pronounced increase in volumetric inclusion of steel fibers. Fiber inclusion typically leads to diminished Poisson's ratio values and restrained lateral deformation in the mortar, attributed to the confining effect exerted by the fibers [17,50]. As the fibers serve as an internal confinement mechanism, the influence of external confinement due to friction at the contact surface of the mortar block and steel platen is proportionally diminished [17].

The bond stress mechanism is characterized by a radial force that pushes against the concrete surrounding the reinforcement. This force generates a hydrostatic radial stress, leading to the development of cylindrical tensile stresses, as illustrated in Figure 13. The magnitude of the resulting constraint effect and wedge generation is primarily governed by two factors: the cover thickness and the tensile capacity of the concrete.

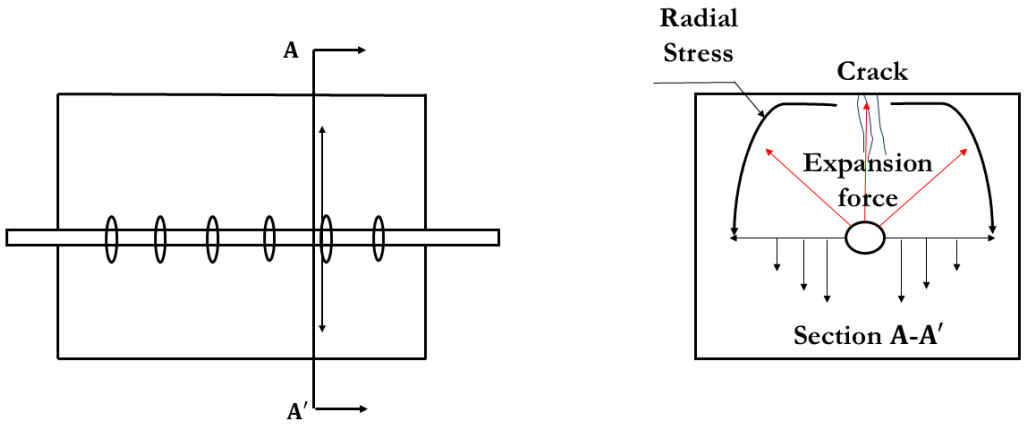

Figure 13. Mechanical interlock between the reinforcement and the surrounding concrete.

4.2.3. The Constitutive Interaction Between Bond Stress and Slip

Typically, the interaction between deformed bars and HPSFRM is evidenced by the measured bond stress and corresponding slip. The average bond stress-slip responses for two different diameters are depicted in Figure 14. A pronounced slip value was noted at the point of maximum bond stress for the 10 mm diameter bar with steel fiber contents of 0% and 1%. The increased slip values are associated exclusively with the prior yielding of the bars. Upon the formation of microcracks, the reinforcing bar began to exhibit gradual slip. The bond-slip response demonstrated an approximately linear increase in load, with minor non-linear behavior observed before the onset of mortar splitting and cracking.

Despite the reduction in bond stress-slip stiffness, the presence of fibers improved the matrix performance by transmitting tensile forces and restraining the progression of crack openings. When the steel fiber content is 1% by volume, the fibers contribute to postponing the crushing of the mortar between the bar lugs, as shown in Figure 10, contributing to enhanced bond strength before reaching the peak load. Reinforcement subjected to pull-out loading tends to exhibit radial expansion. The bond stress-slip relationship reveals that the interface bond stress of deformed reinforcing bars evolves through three characteristic stages. first was the chemical bond strength with no slippage of the reinforcement. Mechanical interlocking is estimated to account for roughly 88% of the adhesive interaction between the ribbed steel rebar and the HPSFRM matrix. There is a friction force between HPSFRM and deformed steel. A distinct post-peak response was not evident in the samples, which may be a consequence of brittle tensile failure behavior characteristic of cement mortar and similar cement-based composites [23,24].

The pronounced post-peak drops in bond stress observed in the pull-out curves highlight the brittle nature of bond failure in specimens without fibers, and 1% of steel fiber cannot prevent this type of sudden drop, especially for larger bar diameters. Under seismic or impact loading, such sudden bond degradation could lead to premature loss of load transfer capacity between reinforcement and the surrounding mortar, thereby reducing the overall energy dissipation of the system. However, the inclusion of more than 1% of steel fibers significantly mitigated this abrupt stiffness loss, as evidenced by the smoother post-peak response [20,30]. The bridging action of the fibers restricted crack propagation, enabling a more gradual reduction in bond resistance and preserving structural integrity even after peak load.

From a practical perspective, this behavior suggests that UHPC and SFRC with steel fibers and enough concrete cover provide enhanced resilience under dynamic loading scenarios. The fibers help to maintain bond continuity after cracking, thereby improving ductility and post-peak energy absorption capacity [14,20]. This is particularly beneficial for masonry elements subjected to seismic or impact forces, if we include more fiber content and enhance the confinement ratio (Cover concrete to bar diameter), where repeated load reversals and stress redistributions occur. Consequently, while plain HPSFRM specimens may be vulnerable to sudden bond degradation, fiber-reinforced specimens are more likely to sustain stable load transfer and delay catastrophic bond failure, ultimately improving the safety and reliability of reinforced masonry structures under extreme loading conditions.

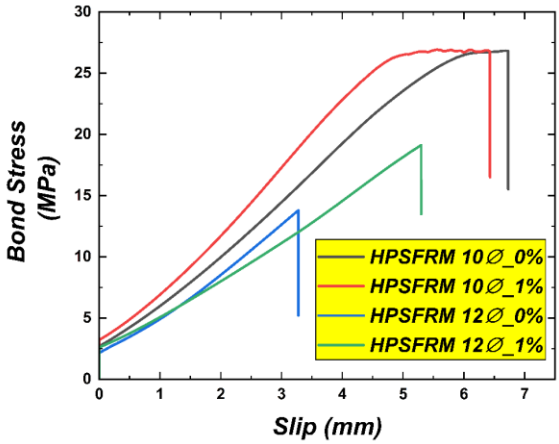

Figure 14. Comparison of bond stress–slip behavior for specimens containing 0% and 1% fiber volume, and 10∅ and 12∅ of a steel bar.

4.3. Assessment of Bond Performance Predicted by Engineering Codes and Standard Equations

The stress transferred at the bond of steel bars and mortar has been predicted by different models over the years [12]. Since no analytical models currently exist to predict the bond strength between steel bars and HPSFRM, the models originally developed for steel bars embedded in concrete were adopted to assess their applicability to cement mortar systems. The comparative analysis presented in this study employs a selection of prominent empirical and code-based Equations (3) and (11) sourced from the literature, encompassing models originally developed for conventional concrete (e.g., Orangun et al. [51], ACI 318 [30]), high-strength concrete [45,52], and fiber-reinforced composites [37]. This diverse selection was intentional, serving to benchmark the performance of High-Performance Steel Fiber-Reinforced Mortar (HPSFRM) against a wide spectrum of existing design tools and to critically evaluate their applicability beyond their original scope. To ensure a consistent and transparent application, specific assumptions were necessitated by the experimental parameters. For models incorporating terms related to transverse reinforcement or bar spacing features absent in the setup, these parameters were set to zero. The actual measured concrete cover was utilized in all calculations, and the concrete compressive strength was directly input from experimental tests on companion specimens. By applying these critical adjustments, this methodology allows for a rigorous assessment of each model's predictive accuracy for HPSFRM.

Several models have been developed and presented as reported in previous studies to estimate the ultimate bond stress values. A typical formulation represents bond stress under the square root of the concrete mean compressive strength, multiplied by a calibration coefficient. This coefficient takes different forms depending on the methodology and underlying assumptions of each proposal. An expression formulated by Orangun et al. [51]. accounts for the interfacial bond strength of steel reinforcement as dependent on whether transverse reinforcement is present or not [39]. The bond stress average at failure was calculated using a regression analysis for bars without the confining action attributable to transverse reinforcement. Equation (3) is as follows.

$$\tau_b = \left(0.10 + 0.25\,\frac{C_{min}}{d_b} + 4.15\frac{d_b}{l_b}\right)\left(f_c^{'}\right)^{0.5} \tag{3}$$

in which C_{min} and $f_c^{'}$ corresponds to the smallest specified cover of the steel reinforcement and the Compressive strength requirement for mortar, correspondingly.

A large-scale database enabled Darwin et al. To estimate the bond strength between ribbed steel rebar and concrete [53]. As revealed by their study, the optimal fitting equation concerning the bonding strength of steel reinforcement without transverse reinforcement was determined in Equation (4), detailed below:

$$\tau_b = [1.5l_d(C_{min} + 0.5d_b) + 51A_b]\left(0.1\frac{C_{max}}{C_{min}} + 0.90\right)\left(f_c^{1^{'}/4}\right)(\pi d_b l_d)^{-1} \tag{4}$$

where C_{max} Corresponds to the greatest of (the underside mortar cover of the ribbed rebar) and (the lesser value between the side mortar cover of the reinforcing bar and half the clear gap separating the bars, augmented by 6.35 mm) and A_b It is the area of the reinforcing bar.

According to Zuo and Darwin [54], the following Equation (5) was derived to describe ribbed rebars not enclosed via transverse reinforcement:

$$\tau_b = [1.43l_d(C_{min} + 0.5d_b) + 56.2A_b](0.1\,\frac{C_{max}}{C_{min}} + 0.90)\,(f_c^{1^{'}/4})\,(\pi d_b l_d)^{-1} \tag{5}$$

According to Chapman and Shah [55], the proposed Equation (6) satisfactorily matches the test results, encompassing pullout failure, mortar splitting, and steel yielding:

$$\tau_b = (0.29 + 0.282\frac{C_{min}}{d_b} + 4.734\frac{d_b}{l_b})(f_c')^{0.5} \quad (6)$$

As prescribed in the ACI design code [30], Equation (7) below was formulated to evaluate the bond strength of ribbed steel embedded within mortar:

$$\tau_b = [1.43 l_b(C_{min} + 0.5\, d_b) + 57.4A_b](0.1\frac{C_{max}}{C_{min}} + 0.90)(\sqrt[4]{f_c'})(\pi d_b l_b)^{-1} \quad (7)$$

Harajli et al. [56] proposed that the empirical Equation (8) below was created from pull-out tests of rebars in SFRC with hooked-end fibers:

$$\tau_b = 2.57\sqrt{f_{cm}} \quad (8)$$

Khaksefidi [57] investigated several variables based on experimental data. The variables that matter are known and remain in Equation (9):

$$\tau_{max} = -40.24219 + 8.07975\sqrt{f_c'} \;;\; R^2 = 0.75 \quad (9)$$

In light of the experimental outcomes, Lee et al. [58] examined how mortar compressive strength up to 90 MPa influences the bond stress of steel reinforcement. To predict the bond stress of steel bars in mortar, the following Equation (10) is provided:

$$\tau_b = 4.1(f_c')^{0.5} \quad (10)$$

From the data obtained through pull-out testing, Hadi [59] developed a model to determine the bond strength between ribbed steel reinforcement and high-strength concrete (HSC). The following Equation (11) is expressed below:

$$\tau_b = 0.083045\sqrt{f_c'}[22.8 - 0.208\left(\frac{c}{d_b}\right) - 38.212\left(\frac{d_b}{l_b}\right)] \quad (11)$$

where τ_b is the Ultimate capacity of bond stress, MPa; f_c indicates the compressive strength measured from mortar cylinders, MPa; c is the minimum mortar cover, mm; d_b indicates the standard diameter of the rebars, mm; and l_b is the Bonded length, mm.

To establish the bond strength of embedded ribbed steel (10 mm diameter) in HPSFRM, as illustrated in Table 6, Equation (9) proves to be more accurate for steel fiber contents of 0% and 1% compared to other equations. Equation (3) has also been shown to be appropriate for estimating the bond strength of 12 mm diameter steel bars, but solely for 0% fiber content. Conversely, Equation (6) accurately predicts the bond strength for 12 mm diameter steel bars with 1% steel fiber content. Equations (3)–(5), (7) and (11) tend to overpredict the bond strength of ribbed steel rebars that have a 10 mm diameter in HPSFRM.

As illustrated in Table 6, the equations uniformly result in underestimations of the bond stress of 12 mm diameter ribbed steel rebars in HPSFRM, except for Equations (5) and (7), demonstrating significant accuracy for the 0% steel fiber content. Compared with the other equations, Equation (11) shows a pronounced tendency to overestimate the bond strength in HPSFRM.

Overall, these results suggest that while some existing bond stress models can provide approximate estimates under limited conditions, they are not universally adaptable to HPSFRM. For smaller bars (10 mm), the majority of Equations (3)–(5), (7) and (11) consistently

overpredicted bond stress by ratios ranging between 1.5 and 2.6 compared with experimental values, reflecting their inability to capture the enhanced confinement and crack-bridging contribution of steel fibers in the high-performance matrix. Only Equation (9) provided bond-to-prediction ratios close to unity (0.93–0.98), demonstrating better adaptability to fiber-reinforced conditions. For larger bars (12 mm), a different trend was observed: most Equations (3), (4), (6), (8), (9) and (10) underestimated bond stress with bond-to-prediction ratios often below 1.0, particularly at 0% fiber, indicating that these formulations do not sufficiently represent the reduced confinement ratio of larger diameters. Equations (5) and (7) were exceptions, showing bond strength ratios close to 1.0 under plain conditions (0% fiber), while Equation (6) showed the best performance for the 12 mm bar with 1% fiber content, suggesting some implicit consideration of confinement effects. This reinforces the conclusion that bond behavior in HPSFRM cannot be reliably predicted using conventional models alone without appropriate calibration.

Table 6. Assessment of Bond Prediction Equations for Steel Reinforcement in HPSFRM.

		Bond Strength Ratio: Experiment/Equation Output								
	Experiment Results	**Equation (3)**	**Equation (4)**	**Equation (5)**	**Equation (6)**	**Equation (7)**	**Equation (8)**	**Equation (9)**	**Equation (10)**	**Equation (11)**
HPSFRM-0-10	25.98	1.53	1.82	1.89	1.25	1.76	1.23	0.98	0.77	2.66
HPSFRM-1-10	26.21	1.50	1.81	1.88	1.23	1.75	1.20	0.93	0.75	2.62
HPSFRM-0-12	13.8	0.91	1.06	1.02	0.74	1.01	0.65	0.52	0.41	1.4
HPSFRM-1-12	19.12	1.22	1.45	1.40	0.99	1.38	0.88	0.7	0.55	1.88
MAE	-	0.29	0.54	0.55	0.18	0.48	0.20	0.25	0.40	1.19
RMSE	-	0.33	0.58	0.59	0.22	0.52	0.25	0.28	0.43	1.24

Note: MAE = Mean Absolute Error; RMSE = Root Mean Square Error. Values calculated based on the absolute error between experimental and predicted bond strength.

The Mean Absolute Error (MAE) and Root Mean Square Error (RMSE) effectively quantify and compare the predictive accuracy of the models. Equation (11) yielded results close to or exceeding unity, indicating that the formulations are appropriate for evaluating the bond strength between cement mortar and steel bars. The superior performance of these models suggests their underlying mechanics, likely their treatment of key parameters like concrete cover and bar diameter, are most transferable to the HPSFRM system, even in the absence of transverse reinforcement.

The systematic overprediction of bond strength by historical models, particularly for larger bar diameters, underscores their fundamental limitation: they were calibrated for plain concrete and cannot capture the unique mechanics of fiber-reinforced mortars. The superior performance of models that account for tensile capacity, however, points toward a viable path forward. This critical gap not only validates the necessity of this study but also definitively justifies the development of new, mechanically grounded equations or fiber-specific modification factors explicitly designed for HPSFRM.

5. Conclusions

Although the bond behavior of steel bars in conventional concrete has been widely investigated, limited research is available on their performance when embedded in high-performance steel fiber-reinforced mortar (HPSFRM). To address this gap, the present study investigates the limited experimental evidence on bond behavior in HPSFRM by conducting standardized pull-out tests across different rebar diameters and fiber contents. Further, it benchmarks the results against several existing prediction models. The parameters examined included bar diameter (10 mm and 12 mm), matrix compressive strength, and steel fiber dosage (0% and 1%). The experimental results were analyzed to identify the governing failure mechanisms and to establish the bond stress–slip relationships for HPSFRM. The key outcomes of this investigation are outlined as follows:

- A notable improvement in bond strength is observed for ribbed steel bars anchored in HPSFRM. According to the mean value obtained from three specimens, the bond strength measured in this study ranged from 19 to 28 MPa.
- Bond failure was significantly affected by the confinement of the bars. Specimens experienced failure by mortar splitting around the bar if the mortar cover thickness was insufficient.
- Bond strength exhibits a declining trend with larger bar diameters, which may be ascribed to the even dispersion of steel fibers employed in the experiment, as well as variations in the height of the ribs. The observed improvement in bond strength and ductility resulting from the addition of 1% steel fibers is a significant outcome, with clear practical implications for the design of precast elements and retrofit strategies in both masonry and high-performance concrete systems.
- The interaction between bond stress and displacement of reinforcing bars anchored in HPSFRM exhibits a pronounced linearity along the ascending branch. An enhanced fiber volume ratio led to augmented bond strength and greater slip at the peak pull-out load, attributable to the enhancement of compressive strength.
- This study provides two key contributions to the field: first, a validated experimental dataset on bond behavior in HPSFRM that benchmarks the effect of fiber content and bar diameter; and second, a critical analytical framework that exposes a significant gap in current design practice. The results unequivocally demonstrate that existing models are ill-suited for HPSFRM, thereby establishing an urgent need for new design equations calibrated for fiber-reinforced systems.
- While this study successfully characterizes the fundamental properties and bond mechanisms of HPSFRM at a component level, the findings are derived from small-scale standardized tests. Consequently, the potential influence of scale effects in larger structural members remains unquantified. Future work will essentially focus on experimental validation through large-scale beam tests and the use of the fundamental parameters obtained here to develop predictive numerical models capable of simulating full-scale structural behavior, thereby facilitating the safe and efficient design of large-scale applications.

Author Contributions: Conceptualization, R.S.A. and S.D.; methodology, R.S.A.; software, R.S.A.; validation, R.S.A. and S.D.; formal analysis, R.S.A.; investigation, R.S.A.; resources, S.D. and M.S.; data curation, R.S.A.; writing—original draft preparation, R.S.A.; writing—review and editing, R.S.A., S.D., M.S., Z.A. and G.M.; visualization, R.S.A.; supervision, S.D.; project administration, S.D. All authors have read and agreed to the published version of the manuscript.

Funding: This research received no external funding.

Data Availability Statement: The raw data supporting the conclusions of this article will be made available by the authors on request.

Conflicts of Interest: The authors declare no conflict of interest.

References

1. Hajar, Z.; Lecointre, D.; Petitjean, J.; Resplendino, J.; Simon, A. Ultra high-performance fiber-reinforced concretes: First recommendations and examples of application. In Proceedings of the fib Symposium on Concrete Structures: The Challenge of Creativity, Avignon, France, 26–28 April 2004.
2. Japan Concrete Institute (JCI). *JCI-S-002-2003*; Method of Test for Load-Displacement Curve of Fiber Reinforced Concrete by Use of Notched Beam. Japan Concrete Institute Standard: Tokyo, Japan, 2003.
3. Bensalem, H.; Djaknoun, S.; Ouedraogo, E.; Amrouche, R. Analysis of thermal-induced spalling tests on high to ultra-high performance concrete subjected to standard fire. *Case Stud. Constr. Mater.* **2021**, *15*, e00704. [CrossRef]

4. Farvees, M.; Raheem, S.; Thamboo, J.; Zahra, T.; Asad, M. Unconfined bond stress and slip characteristics of steel bars embedded in masonry cement mortars. *Case Stud. Constr. Mater.* **2023**, *19*, e02240. [CrossRef]
5. Bae, B.; Choi, H.; Choi, C. Bond stress between conventional reinforcement and steel fiber-reinforced reactive powder concrete. *Constr. Build. Mater.* **2016**, *28*, 176–186.
6. Aïtcin, P.-C. *Binders for Durable and Sustainable Concrete*, 1st ed.; Taylor & Francis: London, UK, 2008.
7. Mehta, P.K.; Monteiro, P.J.M. *Concrete: Microstructure, Properties, and Materials*, 4th ed.; McGraw-Hill: Columbus, OH, USA, 2006.
8. Li, V.C. From Micromechanics to Structural Engineering—The Design of Cementitious Composites for Civil Engineering Applications. *Struct. Eng./Earthq. Eng.* **1991**, *10*, 37–48.
9. Bentur, A.; Mindess, S. *Fibre Reinforced Cementitious Composites*, 2nd ed.; CRC Press: Boca Raton, FL, USA, 2007.
10. Naaman, A.E.; Reinhardt, H.W. High-Performance Fiber-Reinforced Cement Composites: Classification and Applications. *Cem. Concr. Compos.* **2003**, *25*, 529–538.
11. Baran, E.; Akis, T. Pull-out behavior of prestressing strands in steel fiber reinforced concrete. *Constr. Build. Mater.* **2012**, *28*, 362–371. [CrossRef]
12. Golafshani, E.M.; Rahai, A. Bond behavior of steel and GFRP bars in self-compacting concrete. *Constr. Build. Mater.* **2014**, *61*, 230–240. [CrossRef]
13. Tepfers, R. *A Theory of Bond Applied to Overlapped Tensile Reinforcement Splices for Deformed Bars*, 2nd ed.; Chalmers University of Technology of Goteborg: Gothenburg, Sweden, 1973.
14. Liu, H.; Liu, Y.; Li, A.; Lei, H. Experimental study on the bond performance of deformed steel bar in ultrahigh-performance concrete. *Case Stud. Constr. Mater.* **2023**, *18*, e01874. [CrossRef]
15. Eik, M.; Lohmus, K.; Tigasson, M.; Listak, M.; Puttonen, J.; Herrmann, H. DC-conductivity testing combined with photometry for measuring fiber orientations in SFRC. *J. Mater. Sci.* **2013**, *48*, 3745–3759. [CrossRef]
16. Orbe, A.; Cuadrado, J.; Losada, R.; Rojí, E. Framework for the design and analysis of steel fiber reinforced self-compacting concrete structures. *Constr. Build. Mater.* **2012**, *35*, 676–686. [CrossRef]
17. Guler, S.; Akbulut, Z.F. The single and hybrid use of steel and basalt fibers on high-temperature resistance of sustainable ultra-high performance geopolymer cement mortars. *Struct. Concr.* **2023**, *24*, 2402–2419. [CrossRef]
18. Kana, L.; Zhanga, L.; Zhao, Y.; Wu, M. Properties of polyvinyl alcohol fiber reinforced fly ash based engineered geopolymer composites with zeolite replacement. *Constr. Build. Mater.* **2020**, *231*, 117161. [CrossRef]
19. Guler, S.; Akbulut, Z.F. Effect of high-temperature on the behavior of single and hybrid glass and basalt fiber added geopolymer cement mortars. *J. Build. Eng.* **2022**, *57*, 104809. [CrossRef]
20. Hu, A.; Liang, X.; Shi, Q. Bond characteristics between high-strength bars and ultrahigh-performance concrete. *J. Mater. Civil Eng.* **2020**, *32*, 0002919. [CrossRef]
21. Michael, S.; Ekkehard, F. Ultra-high-performance concrete: Research, development and application in Europe. *Acids Spec. Publ.* **2005**, *228*, 51–78.
22. Misnon, M.A.; Giaretton, M.; Ingham, J.; Dizhur, D. Pull-out behaviour of near surface mounted steel wire rope bonded to clay-brick masonry. *Structures* **2021**, *29*, 199–210. [CrossRef]
23. Rodriguez-Mayorga, E.; Hortigon, B.; Ancio, F. Analysis of the main geometrical characteristics that affect the bonding of ribs in rebars thinly covered to repair masonry structures. *Eng. Struct.* **2021**, *246*, 113027. [CrossRef]
24. Fib (International Federation for Structural Concrete). *Fib Model Code for Concrete Structures 2010*; Ernst & Sohn: Berlin, Germany, 2013.
25. Won, J.; Park, C.; Kim, H.; Lee, S.; Jang, C. Effect of fibers on the bonds between FRP reinforcing bars and high-strength concrete. *Compos. Part B* **2008**, *39*, 747–755. [CrossRef]
26. Haddad, R.H.; Shannis, L.G. Post-fire behavior of bond between high-strength pozzolanic concrete and reinforcing steel. *Constr. Build. Mater.* **2004**, *18*, 425–435. [CrossRef]
27. Shi, C.; Wu, Z.; Xiao, J.; Wang, D.; Huang, Z.; Fang, Z. A review on ultra-high-performance concrete: Part I. Raw materials and mixture design. *Constr. Build. Mater.* **2015**, *101*, 741–751. [CrossRef]
28. Teichmann, T.; Schmidt, M. Influence of the Packing Density of Fine Particles on Structure, Strength and Durability of UHPC. In Proceedings of the International Symposium on Ultra-High-Performance Concrete, Kassel, Germany, 13–15 September 2004.
29. Yoo, D.Y.; Shin, H.O.; Yang, J.M.; Yoon, Y.S. Material and bond properties of ultra-high performance fiber-reinforced concrete with micro steel fibers. *Compos. Part B* **2014**, *58*, 122–133. [CrossRef]
30. Darwin, D. *Bond and Development of Straight Reinforcing Bars in Tension; ACI 408-03*; American Concrete Institute: Detroit, MI, USA, 2003; 49p.
31. Krstulovic-Opara, N.; Watson, K.A.; LaFave, J.M. Effect of increased tensile strength and toughness on reinforcing-bar bond behavior. *Cem. Concr. Res.* **1994**, *16*, 129–141. [CrossRef]
32. Liu, P.; Tang, J.P.; Feng, R.; Fan, Y.; Zhu, J.H. Interfacial behaviour and shear performance of polarized CFRCM-strengthened corroded RC continuous beams. *Constr. Build. Mater.* **2025**, *472*, 140786. [CrossRef]

33. Liu, P.; Tang, J.P.; Feng, R.; Fan, Y.; Zhu, J.H. Tensile behavior and flexural performance of polarized CFRCM-strengthened corroded RC continuous beams. *Constr. Build. Mater.* **2025**, *76*, 109022. [CrossRef]
34. Tang, J.P.; Feng, R.; Quach, W.M.; Zeng, J.J. Axial compressive behaviour of simulated corrosion-damaged RC columns retrofitted with UHPFRC jackets subjected to dry-wet cycling condition. *Structures* **2024**, *424*, 135956. [CrossRef]
35. *NF EN 197-1*; Cement Part 1. Composition, Specifications and Conformity Criteria for Common Cements. AFNOR/CEN: Brussels, Belgium, 2012.
36. Tang, J.P.; Feng, R.; Quach, W.M. Evaluation of flexural performance on corrosion-damaged RC beams retrofitted with UHPFRCC under marine exposure. *Eng. Struct.* **2025**, *333*, 120193. [CrossRef]
37. *EN 196-1*; Methods of Testing Cement Part 1: Determination of Strength. CEN: Brussels, Belgium, 2016.
38. *NF EN 934-2*; Admixtures for Concrete, Mortar and Grout Part 2: Concrete Admixtures—Definitions, Requirements, Conformity, Marking and Labelling. AFNOR/CEN: Brussels, Belgium, 2009.
39. Djaknoun, S.; Ouedraogo, E.; Benyahia, A.A. Characterisation of the behaviour of high-performance mortar subjected to high temperatures. *Constr. Build. Mater.* **2012**, *28*, 176–186. [CrossRef]
40. Yazıcı, S.; Arel, H.S. The effect of steel fiber on the bond between concrete and deformed steel bars in SFRCs. *Constr. Build. Mater.* **2013**, *40*, 299–305. [CrossRef]
41. RILEM. Technical Recommendations for the testing and use of construction materials. In *RC6 Bond Test for Reinforcement Steel, Pull-Out Test*; RILEM: Champs-sur-Marne, France, 1994; Volume 2.
42. *EN 12390-1*; Testing Hardened Concrete Part 1: Shape, Dimensions and Other Requirements for Specimens and Moulds. CEN: Brussels, Belgium, 2021.
43. Xiao, J.; Falkner, H. Bond behavior between recycled aggregate concrete and steel rebars. *Constr. Build. Mater.* **2007**, *21*, 395–401. [CrossRef]
44. Lemnitzer, L.; Schröder, S.; Lindorf, A.; Curbach, M. Bond behavior between reinforcing steel and concrete under multiaxial loading conditions in concrete containments. In Proceedings of the 20th International Conference on Structural Mechanics in Reactor Technology (SMiRT 20), Espoo, Finland, 9–14 August 2009; p. 1734.
45. Al-Shannag, M.J.; Charif, A. Bond behavior of steel bars embedded in concretes made with natural lightweight aggregates. *J. King Saud Univ.—Eng. Sci.* **2017**, *29*, 365–372. [CrossRef]
46. Deng, Z.; Yuan, C. Experimental study on bond capability between high-strength bar and reactive powder concrete. *China Civ. Eng. J.* **2014**, *47*, 69–78.
47. Lagier, F.; Massicotte, B.; Charron, J.P. Experimental investigation of bond stress distribution and bond strength in unconfined UHPFRC lap splices under direct tension. *Cem. Concr. Compos.* **2016**, *74*, 26–38. [CrossRef]
48. Irshidat, M.R. Bond strength evaluation between steel rebars and carbon nanotube-modified concrete. *Case Stud. Constr. Mater.* **2021**, *14*, e00477. [CrossRef]
49. Rafi, M.M. Study of bond properties of steel rebars with recycled aggregate concrete. Analytical Modeling. *Strength Mater.* **2019**, *51*, 166–174. [CrossRef]
50. Rafi, M.M. Study of bond properties of steel rebars with recycled aggregate concrete. Experimental Testing. *Strength Mater.* **2018**, *50*, 937–950. [CrossRef]
51. Orangun, C.O.; Jirsa, J.O.; Breen, J.E. A reevaluation of test data on development length and splices. *ACI Mater. J.* **1977**, *74*, 114–122.
52. Gesoglu, M.; Güneyisi, E.; Alzeebaree, R.; Mermerda, K. Effect of silica fume and steel fiber on the mechanical properties of the concretes produced with cold bonded fly ash aggregates. *Constr. Build. Mater.* **2013**, *40*, 982–990. [CrossRef]
53. Darwin, D.; Tholen, M.L.; Idun, E.K.; Zuo, J. Splice strength of high relative rib area reinforcing bars. *ACI Struct. J.* **1996**, *93*, 95–107. [CrossRef]
54. Zuo, J.; Darwin, D. Splice strength of conventional and high relative rib area bars in normal and high-strength concrete. *ACI Struct. J.* **2000**, *97*, S65. [CrossRef]
55. Chapman, R.A.; Shah, S.P. Early-age bond strength in reinforced concrete. *ACI Mater. J.* **1988**, *84*, 501–510.
56. Harajli, M.H.; Salloukh, K.A. Effect of fibers on development/splice strength of reinforcing bars in tension. *ACI Mater. J.* **1997**, *94*, 317–324. [CrossRef]
57. Khaksefidi, S.; Ghalehnovi, M.; Brito, J.D. Bond behavior of high-strength steel rebars in normal (NSC) and ultra-high performance concrete (UHPC). *J. Build. Eng.* **2021**, *33*, 101592. [CrossRef]
58. Lee, J.Y.; Kim, T.Y.; Kim, T.J.; Yi, C.K.; Park, J.S.; You, Y.C.; Park, Y.H. Interfacial bond strength of glass fiber reinforced polymer bars in high-strength concrete. *Compos. Part B* **2008**, *39*, 258–270. [CrossRef]
59. Hadi, M.N.S. Bond of high-strength concrete with high-strength reinforcing steel. *Open Civil Eng. J.* **2008**, *2*, 143–147. [CrossRef]